Journal Pre-proof

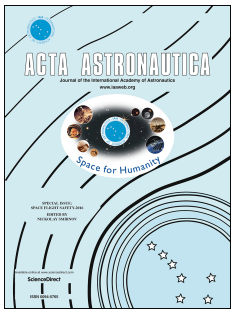

Adaptive Sliding Mode Control for Deployment of Electro-dynamic Tether via Limited Tension and Current

Shumin Chen, Aijun Li, Changqing Wang, Chenguang Liu

PII: S0094-5765(19)31458-4

DOI: https://doi.org/10.1016/j.actaastro.2019.12.025

Reference: AA 7808

To appear in: *Acta Astronautica*

Received Date: 31 July 2019

Revised Date: 8 December 2019

Accepted Date: 19 December 2019

Please cite this article as: S. Chen, A. Li, C. Wang, C. Liu, Adaptive Sliding Mode Control for Deployment of Electro-dynamic Tether via Limited Tension and Current, *Acta Astronautica*, https://doi.org/10.1016/j.actaastro.2019.12.025.

Adaptive Sliding Mode Control for Deployment of Electro-dynamic Tether via Limited Tension and Current

Shumin Chen*, Aijun Li, Changqing Wang, Chenguang Liu

School of Automation, Northwestern Polytechnical University, 1 Dongxiang Road, Chang'an District, Xi'an Shaanxi, 710129, P.R. China
* Corresponding Author. E-mail address: chenshumin@mail.nwpu.edu.cn

Abstract

This paper studies the deployment control of the electrodynamic tether system by means of tether tension and electric current regulation. Design of the control strategy has been implemented based on the simplified dumbbell model. In order to improve the robustness of the control system to the possible external disturbances, an adaptive sliding mode control is proposed to deploy the tether to the local vertical with the consideration of input limitations, which are introduced by a pair of saturation functions to ensure that the tether tension is always non-negative and the current is within limits. In addition, the proposed adaptive law is intended to estimate the mass parameter of the model, which is with uncertainty caused by the difficulty in accurately determining the masses of the end-bodies. The stability characteristic of the system under the proposed hybrid controller is studied based on the Lyapunov theory. Numerical case studies in the different orbital inclinations are conducted to illustrate the effectiveness of the proposed control strategy. Moreover, the performance of the controller is presented in the presence of the initial perturbations, the external disturbances and the uncertainty of mass parameter of the system.

Keywords: Electro-dynamic tether; Deployment control; Sliding mode control; Adaptive law

Nomenclature

$\boldsymbol{B}$	=	Magnetic field of Earth
C	=	Center of Mass (CM) of the system
I	=	Electric current along electro-dynamic tether
i	=	Orbital inclination
l	=	Tether length
m_1, m_2	=	Mass of end-bodies
Q_θ	=	Generalized force for in-plane angle
Q_β	=	Generalized force for out-plane angle
$\boldsymbol{r}_c$	=	Orbital radius of the CM of the system
$\boldsymbol{T}$	=	Tether tension
β	=	Out-plane angle
$\boldsymbol{\Delta}$	=	The disturbances acting on the system
σ	=	Argument of latitude
θ	=	In-plane angle
ϑ	=	True anomaly
μ_e	=	Coefficient of Earth's gravity field

μ_m = Magnetic moment of the Earth's dipole
Ω = Angular velocity of the circular orbit
Ω_a = Right ascension of ascending node (RAAN)
ω = Orbital angular velocity
ω_p = Argument of perigee

1. Introduction

Space Tether System (STS) refers to a combination of several spacecrafts connected by tethers, tapes, or wires [1]. In recent years, tether application has been considered as a quite promising branch of space explorations, such as atmosphere explorations and orbital maneuvers, for the tether system can guarantee a long operating distance and provide the possibility to complete missions without fuel consumption by means of momentum exchange, which shows the unique superiority of tether systems compared to conventional spacecraft systems [2,3]. Besides, debris deorbiting [4], formation flying [5], payload capture [6], and tethered robot [7] based on STS technology have also been discussed theoretically and partially certificated by ground or space experiments over the past decades.

STS with conductive tethers or tapes is also known as Electrodynamic Tether (EDT) system. The EDT system has shown its broad application prospects in space missions around Earth; notably, bare tether gains much attention as it can collect electrons from the rarefied ionosphere more efficiently [8]. There are also some works studied on the use of electrodynamic tethers for missions around other planets such as Jupiter [9]. It is expected that the Lorenz force generated by the motion of conductive tether in geomagnetic field can be used as a thruster, which provides the ability to change orbit altitude of a spacecraft in Low Earth Orbit (LEO). Many researchers have focused on the application of EDT for debris de-orbit, and the relevant modeling, dynamics analysis, and control problems are studied. Atashgah and Gazerpour et al [4] worked on the time-optimal de-orbit control by limited current regulation. Xu and Kong [10] established a rigid bar model and a flexible cable model in their work, and it can be seen from the comparison of different models that the rigid rod model has theoretical rationality, and the flexible model is more in accordance with the deformation characteristics of the EDT under Ampere force. It is worth noting that when current starts flowing along tether, the stable equilibrium position in the local vertical no longer exists, and the dynamic behaviors of the EDT system exhibit periodic solutions or rather dynamic instability, which requires proper control schemes [11]. Zhong and Zhu [12] proposed a controller based on the roll angle feedback to keep libration angles bounded through current switching. Kojima and Sugimoto [13] studied the nonlinear libration control issue for EDT systems comprised of one main satellite and two subsatellites. Afterwards, two time-delayed feedback control methods were applied to deal with the librations of EDT systems in frozen inclined elliptic orbits [14]. The foregoing studies demonstrated that electrodynamic force can be regarded as a control force to damp the librations of system.

The successful deployment of tether is a pre-condition for any space tether mission. Although many works have been devoted to the deployment dynamics and control issues of tethered systems [15,16,17], challenge remains in the design of non-thrusted tether deployment [18]. A common operation mode for an EDT system is to keep the tether non-current carrying in deployment process and energize the fully-deployed conductive tether in de-orbit process. In this way, the deployment issue of EDT is actually equivalent to the deployment of non-conductive STS,

on which significant research efforts have been concentrated in order to control the libration motion with the end mass on the tether deployed to a desired position in a fast and stable manner by means of pure tension, or tension-thruster strategies [19,20,21]. It is well-known that libration motion should be considered and controlled during deployment to ensure the success of missions. Although the abovementioned control schemes have demonstrated their validity, the possibility of non-propellant consumption and the potential of electrodynamic force for stabilizing libration motion in deployment are often ignored. It is noticeable that the attitude motion of the tether will be influenced by the excitation of electrodynamic force [22], which makes the deployment more complicated, but provides possibilities for the electrodynamic force to be used as a kind of control force. A hybrid control strategy based on tether tension and electrodynamic force fully exploits this possibility and shows its superiority in reducing the maximum in-plane angle in deployment [23]. Huang and Liu [24] investigated the hybrid control for the underactuated deployment issue of EDT systems by using the backstepping method. Wen and Jin et al [25] studied the three-dimensional deployment of EDT systems, and developed a feedback controller with the consideration of the constraints of tether tension and current using a pair of saturation functions. Luo and Wen et al [26] proposed control laws of current switching to dissipate the libration energy during three-dimensional deployment of EDT systems. As indicated in the aforementioned studies concerning a hybrid control strategy in EDT deployment, the combination of tether tension and electric current can facilitate the libration control during the deployment process [25-26]. However, to the best knowledge of the authors, further research on EDT deployment is needed, when model uncertainty and the external disturbances acting on the system are taken into consideration, which is the motivation of the present paper.

This paper studies the control issue of EDT deployment via the regulation of tether tension and electric current, taking into consideration the external disturbances and the unknown mass parameter that might be encountered in EDT missions. In order to improve the anti-interference ability of the system, an adaptive sliding mode control is adopted in this paper, which has been proven to be an effective method for coping with model uncertainty. The following sections are organized as follows: in Section 2 the dynamic model of the EDT system is introduced; the controller design and stability analysis are given in Section 3; numerical case studies in Section 4 illustrate the performance of the proposed controller, and conclusions are drawn in Section 5.

2. Mathematical modeling

The diagram of the EDT system is shown in Fig. 1. In the current work, m_1 represents the mass of the main satellite, and m_2 represents the mass of the subsatellite, which is usually equipped with a cathode emitter to realize charge exchange with the space plasma environment.

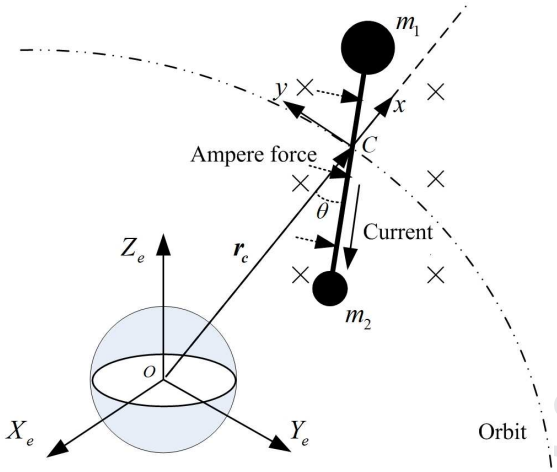

Fig. 1. The diagram of the EDT system

The coordinate systems $OX_eY_eZ_e$ and $Cxyz$ shown in Fig. 1 are ECI (Earth-centered inertia) frame and LVLH (Local Vertical Local Horizontal) frame, respectively. The origin of $OX_eY_eZ_e$ is located at the mass center of the Earth, and the OX_e axis points to the Vernal Equinox; the OZ_e axis aligns with the rotation axis of the Earth. The orbital frame LVLH is used to describe the libration motion of the EDT system, in which the origin C is located at the CM of the system, with the Cx axis along the local vertical pointing towards the Zenith, and the Cy axis aligning along the velocity direction of the CM of the system.

Assumptions. For the convenience of modeling, some assumptions are made in this work: 1) The simplified dumbbell model is adopted, where the end-bodies are regarded as lumped masses and the tether slack configurations are not considered. 2) The mass of tether can be omitted in deployment due to that it is always tiny compared to the masses of end-bodies. 3) The orbit motion of the EDT system remains unaffected during the deployment process.

Remark 1. Note that the deployment time needed in tether missions is usually short, it is reasonable to assume that the orbit of system during tether deployment remains unchanged with no consideration of perturbations. Take the YES-2 mission as an example. It can be seen from the results of the mission that the total deployed length in the first deployment stage is 3378m, and the time needed in this stage is only 5580s [27], which is approximately one orbit period (Note that the mission was built to operate from a platform called Foton-M3, the orbit altitude of which is about 280km).

Considering the assumptions above, the equations of dynamic model can be written as follows based on Lagrangian mechanics [25]:

$$\ddot{l} - l[\dot{\beta}^2 + (\dot{\theta}+\omega)^2\cos^2\beta + (1+e\cos\vartheta)^{-1}\omega^2\left(3\cos^2\theta\cos^2\beta - 1\right)] = \frac{-T}{m_e} \tag{1a}$$

$$\ddot{\theta} + \dot{\omega} + 2\left(\dot{\theta}+\omega\right)\left(\frac{\dot{l}}{l} - \dot{\beta}\tan\beta\right) + 1.5(1+e\cos\vartheta)^{-1}\omega^2\sin 2\theta = \frac{Q_\theta}{m_e l^2\cos^2\beta} \tag{1b}$$

$$\ddot{\beta} + 2\dot{\beta}\frac{\dot{l}}{l} + \sin\beta\cos\beta\left[\left(\dot{\theta}+\omega\right)^2 + 3(1+e\cos\vartheta)^{-1}\omega^2\cos^2\theta\right] = \frac{Q_\beta}{m_e l^2} \tag{1c}$$

where $m_e = \dfrac{m_1 m_2}{m_1 + m_2}$ represents the mass parameter of the system.

Furthermore, when the system runs in a circular orbit, ω can be replaced by the orbital angular velocity Ω, thus Eq. (1) can be simplified further:

$$\ddot{l} - l[\dot{\beta}^2 + (\dot{\theta} + \Omega)^2 \cos^2\beta + \Omega^2\left(3\cos^2\theta\cos^2\beta - 1\right)] = \frac{-T}{m_e} \tag{2a}$$

$$\ddot{\theta} + 2\left(\dot{\theta} + \Omega\right)\left(\frac{\dot{l}}{l} - \dot{\beta}\tan\beta\right) + 1.5\Omega^2 \sin 2\theta = \frac{Q_\theta}{m_e l^2 \cos^2\beta} \tag{2b}$$

$$\ddot{\beta} + 2\dot{\beta}\frac{\dot{l}}{l} + \sin\beta\cos\beta\left[\left(\dot{\theta} + \Omega\right)^2 + 3\Omega^2\cos^2\theta\right] = \frac{Q_\beta}{m_e l^2} \tag{2c}$$

where $\Omega = \sqrt{\mu_e / r_c^3}$.

In the current work, we adopt the non-titled dipole model to depict the Earth's geomagnetic field [28], which can be expressed as follows in the orbital frame:

$$\boldsymbol{B} = \begin{bmatrix} B_x \\ B_y \\ B_z \end{bmatrix} = \begin{bmatrix} -2\dfrac{\mu_m}{r_c^3}\sin i \sin\sigma \\ \dfrac{\mu_m}{r_c^3}\sin i\cos\sigma \\ \dfrac{\mu_m}{r_c^3}\cos i \end{bmatrix} \tag{3}$$

where B_x, B_y, B_z represent the components of $\boldsymbol{B}$ with respect to the axes of $Cxyz$, respectively.

Moreover, the generalized electrodynamic forces can be evaluated by means of the virtual work principle:

$$Q_\theta = \frac{I(m_1 - m_2)}{2(m_1 + m_2)} l^2 \cos\beta\left[\sin\beta\left(B_y\sin\theta + B_x\cos\theta\right) - B_z\cos\beta\right] \tag{4a}$$

$$Q_\beta = \frac{I(m_1 - m_2)}{2(m_1 + m_2)} l^2\left(B_y\cos\theta - B_x\sin\theta\right) \tag{4b}$$

3. Controller design and stability analysis

In this section, a sliding model controller is derived to control the deployment process of the EDT system. With the addition of robust terms, the control system can show a good performance with regard to the robustness of system [29]. To deal with the model uncertainty, an adaptive control law and its modification are addressed, which has the ability to change its parameters as the controlled object changes. The proposed adaptive sliding model controller in the present work is intended to adapt the mass parameter of the EDT system during deployment, which is necessary because this parameter may be unknown, which can be accounted for by that the masses of the end-bodies cannot always be determined accurately in practical missions due to a variety of reasons, such as fuel consumption.

3.1 Controller design

Set the state vector of the system as $\boldsymbol{x}=[l,\dot{l},\theta,\dot{\theta},\beta,\dot{\beta}]^T$, and for the convenience of controller design, the dynamic model of EDT in Eq. (2) is reshaped as follows:

$$m_e\ddot{l}=m_e f_1(\boldsymbol{x})+u_1+\Delta_1 \tag{5a}$$

$$\ddot{\theta}=f_2(\boldsymbol{x})+g_1(\boldsymbol{x})u_2+\Delta_2 \tag{5b}$$

$$\ddot{\beta}=f_3(\boldsymbol{x})+g_2(\boldsymbol{x})u_2+\Delta_3 \tag{5c}$$

with

$$f_1(\boldsymbol{x})=l[\dot{\beta}^2+(\dot{\theta}+\Omega)^2\cos^2\beta+\Omega^2\left(3\cos^2\theta\cos^2\beta-1\right)],$$

$$f_2(\boldsymbol{x})=-2\left(\dot{\theta}+\Omega\right)\left(\frac{\dot{l}}{l}-\dot{\beta}\tan\beta\right)+1.5\Omega^2\sin 2\theta,$$

$$f_3(\boldsymbol{x})=-2\dot{\beta}\frac{\dot{l}}{l}+\sin\beta\cos\beta\left[\left(\dot{\theta}+\Omega\right)^2+3\Omega^2\cos^2\theta\right],$$

$$g_1(\boldsymbol{x})=\frac{(m_1-m_2)}{2m_e\cos\beta(m_1+m_2)}\left[\sin\beta\left(B_y\sin\theta+B_x\cos\theta\right)-B_z\cos\beta\right],$$

$$g_2(\boldsymbol{x})=\frac{(m_1-m_2)}{2m_e(m_1+m_2)}\left(B_y\cos\theta-B_x\sin\theta\right).$$

where $u_1=-T$, $u_2=I$ represent the control inputs; m_e is regarded as an unknown parameter, which is needed to be estimated; $\boldsymbol{\Delta}=[\Delta_1,\Delta_2,\Delta_3]^T$ represents the total external disturbances acting on the system, which are mainly caused by the solar radiation pressure, the aerodynamic torque and the gradient torque [30]. Besides, Δ_1 stands for disturbance force and Δ_2, Δ_3 are angular accelerations.

Remark 2. As for the range of orbital altitude which is concerned in this paper, namely, for the LEO, the environmental disturbances can be regarded as bounded. Consequently, it is reasonable to set $|\boldsymbol{\Delta}|\le D$, where D is a positive number and represents the boundary. Besides, though the mass parameter m_e is unknown, it is still obvious that the parameter has the relationship $m_e>0$, and usually it is easy to obtain the range of this parameter: $m_{\min}\le m_e\le m_{\max}$.

The control issue in the current work is to deploy the tether to the desired local vertical, which is an equilibrium position for the non-conductive space tether system. Although equilibrium positions have no existence for system under the action of Ampere force, the vertical position still has important reference value for EDT missions. In this regard, the terminal states are defined as $\boldsymbol{x}_k=[l_k,\dot{l}_k,\theta_k,\dot{\theta}_k,\beta_k,\dot{\beta}_k]^T$, and except for the tether length, the final values of all the other states approach to zero.

The sliding mode surface is defined as:

$$\begin{cases} s_1 = \dot{e}_1 + c_1 e_1 = x_2 - q \\ q = \dot{x}_{1k} - c_1 e_1 \end{cases} \tag{6}$$

where $e_1 = x_1 - x_{1k}$ denotes the tracking error of tether length.

The tension control law is given in the following form:

$$u_1 = \hat{m}_e \dot{q} - \hat{m}_e f_1(x) - k_s s_1 - \eta_1 \operatorname{sgn}(s_1) \tag{7}$$

where $\hat{m}_e$ represents the estimated value of the mass parameter, and $\hat{m}_e \dot{q}$ denotes the adaptive compensation; $-\eta_1 \operatorname{sgn}(s_1)$ reflects the robustness of the control law; k_s and η_1 are the parameters of the controller, and satisfy: $k_s > 0$, $\eta_1 \geq D$, respectively.

Note that the chattering will be obvious when the uncertainty of mass parameter in the model is large, the switching function in the controller is replaced with a saturation function to prevent the chattering:

$$u_1 = \hat{m}_e \dot{q} - \hat{m}_e f_1(x) - k_s s_1 - \eta_1 sat(s_1) \tag{8}$$

where the saturation function is described as:

$$sat(s_1) = \begin{cases} 1, & s_1 > \chi \\ k s_1, & |s_1| \leq \chi \\ -1, & s_1 < -\chi \end{cases} \tag{9}$$

where χ represents the thickness of the boundary layer, and $k = \frac{1}{\chi}$.

Similarly, u_2 is derived as:

$$u_2 = \frac{1}{g_1(x)}(-f_2(x) + \dot{x}_{4k} + c_2 \dot{e}_2 + \eta_2 sat(s_2)) \tag{10}$$

where $s_2 = \dot{e}_2 + c_2 e_2$, and $e_2 = x_3 - x_{3k}$ denotes the tracking error of the in-plane angle; $sat(s_2)$ has the same form as the saturation function $sat(s_1)$; c_2, η_2 are the parameters of the controller.

3.2 Stability analysis

The stability of the proposed controller can be proved by the Lyapunov function, which is defined as follows:

$$V_1 = \frac{1}{2} m_e s_1^2 + \frac{1}{2\gamma} \tilde{m}_e^2 \tag{11}$$

where $\gamma > 0$, and $\tilde{m}_e = \hat{m}_e - m_e$ denotes the estimation error for m_e.

Then, take the derivative of V_1:

$$\begin{aligned}\dot{V}_1 &= m_e s_1 \dot{s}_1 + \frac{1}{\gamma}\tilde{m}_e \dot{\hat{m}}_e \\ &= s_1\left(m_e \dot{x}_2 - m_e \dot{q}\right) + \frac{1}{\gamma}\tilde{m}_e \dot{\hat{m}}_e \\ &= s_1\left(m_e f_1(x) + u_1 + \Delta_1 - m_e \dot{q}\right) + \frac{1}{\gamma}\tilde{m}_e \dot{\hat{m}}_e \\ &= s_1\left(-\tilde{m}_e f_1(x) + \tilde{m}_e \dot{q} - k_s s_1 - \eta_1 sat(s_1) + \Delta_1\right) + \frac{1}{\gamma}\tilde{m}_e \dot{\hat{m}}_e \\ &= s_1\left(-k_s s_1 - \eta_1 sat(s_1) + \Delta_1\right) + \tilde{m}_e\left(-s_1 f_1(x) + s_1 \dot{q} + \frac{1}{\gamma}\dot{\hat{m}}_e\right)\end{aligned} \tag{12}$$

Hereby, the adaptive law $\dot{\hat{m}}_e$ is proposed as the following form:

$$\dot{\hat{m}}_e = \gamma s_1\left(f_1(x) - \dot{q}\right) \tag{13}$$

where γ represents the parameter of the adaptive law.

Furthermore, substituting the adaptive law into $\dot{V}_1$, one has:

$$\dot{V}_1 = -k_s {s_1}^2 - \eta_1 |s_1| + \Delta_1 s_1 < -k_s {s_1}^2 \le 0 \tag{14}$$

Given the fact that the control input u_1 is tether tension, which is limited physically because of the characteristics of the tether, it is necessary to limit the boundary of the adaptive law, which will affect the value of the control input according to Eq. (7). Therefore, the adaptive law is modified as follows [29]:

$$\dot{\hat{m}}_e = \begin{cases} 0, & if\ \hat{m}_e = m_{\min}\ and\ \dot{\hat{m}}_e < 0 \\ 0, & if\ \hat{m}_e = m_{\max}\ and\ \dot{\hat{m}}_e > 0 \\ \gamma s_1\left(f_1(x) - \dot{q}\right), & otherwise \end{cases} \tag{15}$$

where $m_{\max}$ and $m_{\min}$ are the parameters of the modified adaptive law.

Similarly, define V_2 as:

$$V_2 = \frac{1}{2}{s_2}^2 \tag{16}$$

And the derivative of V_2 satisfies:

$$\dot{V}_2 = -s_2 \Delta_2 - \eta_2 |s_2| \le 0 \tag{17}$$

Hence, the closed-loop system is asymptotically stable according to La Salle's invariance principle since $\dot{V}_1$ and $\dot{V}_2$ are negative semi-definite [31].

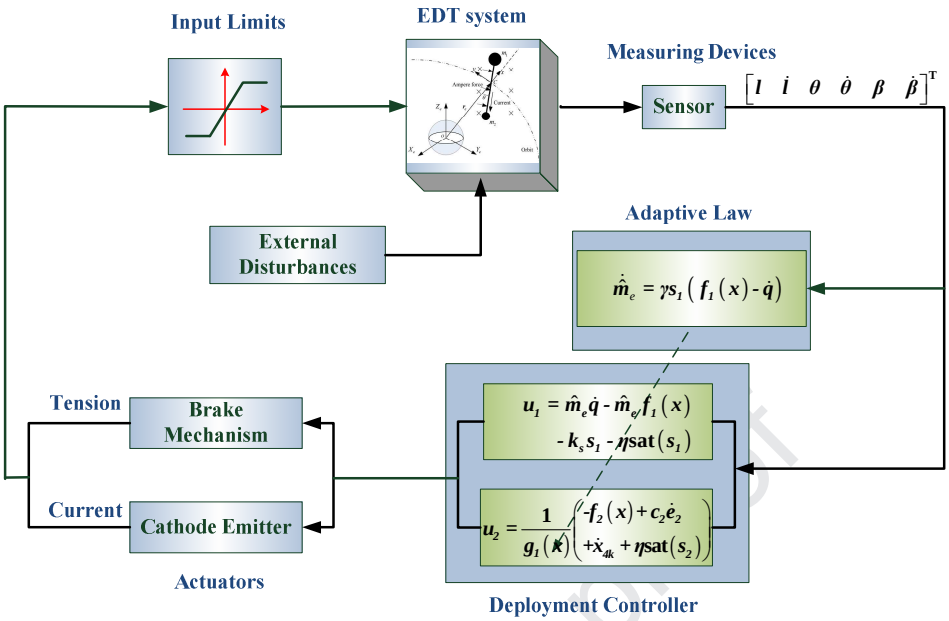

Fig. 2. The block diagram of the adaptive sliding mode control scheme

4. Numerical simulations and discussions

The numerical simulations and analysis on a representative EDT system are carried out in this section to verify the effectiveness and robustness of the proposed control scheme, which is illustrated in Fig. 2.

4.1 Parameters setting

The physical parameters of the EDT system are selected as: $m_1 = 1000\text{kg}$, $m_2 = 50\text{kg}$, $h = 500\text{km}$, $\omega_p = 0\text{rad}$, and $\Omega_a = 0\text{rad}$. The initial conditions are given as: $l(0) = 0.5\text{m}$, $\theta(0) = \beta(0) = 0\text{rad}$, $\dot{l}(0) = 1.5\text{m/s}$, $\dot{\theta}(0) = \dot{\beta}(0) = 0\text{rad/s}$; and the desired deployment states are: $l_k = 3000\text{m}$, $\dot{l}_k = 0\text{m/s}$, $\theta_k = 0\text{rad}$, $\dot{\theta}_k = 0\text{rad/s}$.

According to [30], the magnitudes of the aforementioned primary disturbances acting on spacecrafts in LEO are in the range of 1×10^{-5}. Considering the dynamic model of EDT shown in Eq. (5) is dimensional, the disturbance force Δ_1 can be set as the maximum of the range, that is, $\Delta_1 = 1\times10^{-5}\text{N}$. Furthermore, the angular accelerations caused by the disturbance torques can be evaluated as: $\Delta_2 \approx \Delta_3 = 8.4\times10^{-7}\ \text{rad/s}^2$. Besides, due to the difficulty of explicitly modelling for external disturbances [20], it is widely adopted to describe disturbances as a set of periodic functions. As a result, the disturbances can be expressed as follows: $\Delta_1(t) = 1\times10^{-5}\sin(200\Omega t)\text{N}$, $\Delta_2(t) \approx \Delta_3(t) = 8.4\times10^{-7}\sin(200\Omega t)\text{rad/s}^2$. Based on the discussions above, the boundary of Δ can be set as: $D = 0.01$, which is larger than the upper value of the disturbances to guarantee a higher ability of anti-disturbance.

The restricted conditions for the control inputs T and I are: $0.1\text{N} \le T \le 1\text{N}$, $|I| \le 2\text{A}$, respectively. The parameters of the modified adaptive law are: $\gamma = 0.0081$, $m_{\max} = 50$, $m_{\min} = 45$, and the initial value of the adaptive law is selected as: $\hat{m}_e(0) = 48.5$. When selecting parameters for the SMC controllers, there are some guidelines that

need to be concerned about. Take the controller u_1 as an example. The parameter of the controller k_s determines the convergence rate of the system, and the parameter η_1 represents the velocity of the approach law of sliding surface. Note that if the velocity of approaching is too large, then the chattering will increase, which is undesirable in practice, because it may result in lower control accuracy and excite high-frequency dynamics of the system. In order to improve the convergence rate and weaken chattering, k_s can be chosen larger and η_1 should be smaller under the foregoing constraints $k_s > 0$, $\eta_1 \geq D$. Given these concerns, in the simulations the parameters of the controllers are set as follows: as for u_1, one has $c_1 = 0.001$, $k_s = 0.5$, $\eta_1 = 0.01$, and the thickness of the boundary layer of the saturation function is $\chi = 0.001$; for u_2, one has $c_2 = 25000$, and the other parameters are the same as for u_1 accordingly.

4.2 Case studies

Considering the orbit inclination will affect the motion of the EDT system, three cases under the different inclinations are studied in this subsection. Note that the geomagnetic field model adopted in this paper is non-titled dipole model, that is, the angle between the Earth's rotation axis and the Earth's dipole axis is ignored. In this way, when the orbital inclination is close to 90^o, such as polar orbits or Sun-synchronous orbits, the generated electrodynamic force is weak, which might not be sufficient to be regarded as a control force. With these considerations in mind, the inclinations chosen for evaluation are 0, 15^o and 60^o, which can respectively represent the equatorial plane, low orbital inclination and large orbital inclination to some extent. The simulation time in the studied cases is the actual running time of the EDT system in orbit, which is set as $t = 10000\text{s}$. The simulation results are shown in the following figures.

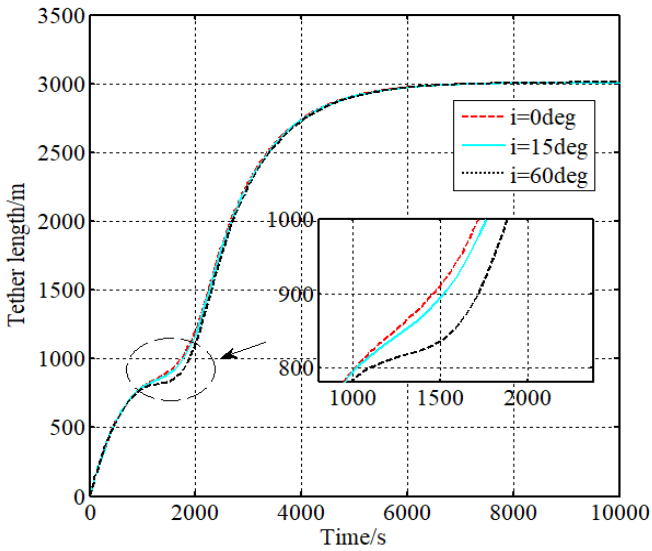

Fig. 3. Variation curves of the EDT length versus time

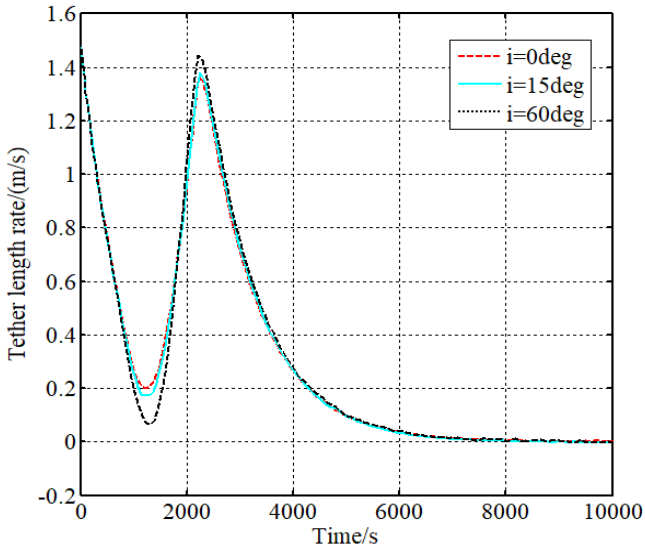

Fig. 4. Variation curves of the EDT length rate versus time

Fig. 3 and Fig. 4 depict the time histories of the tether length and its rate in the case of different orbital inclinations. In general, the curves of the tether length and its rate in the three cases are basically coincide. As shown in Fig. 3, the tether can be deployed from the initial length (0.5m) to the commanded length (3000m), and the deployment time required is about 7660s, which is equal to 1.35 orbit times approximately. Moreover, the inset in Fig. 3 demonstrates that the curves of the tether length are smoother when the inclinations are lower. Besides, there is no overshoot in the variation curves of the tether length, which meets the expectations of deployment missions. As seen from Fig. 4, there are no violent fluctuations in the curves of the tether length rate, and the deployment velocity is always larger than zero (the magnitude of the maximum velocity is about 1.4m/s), which indicates that there is no tether winding during deployment, and the safety of the process can be guaranteed. Therefore, it can be concluded that the control law is successful in the three cases to achieve a stable deployment.

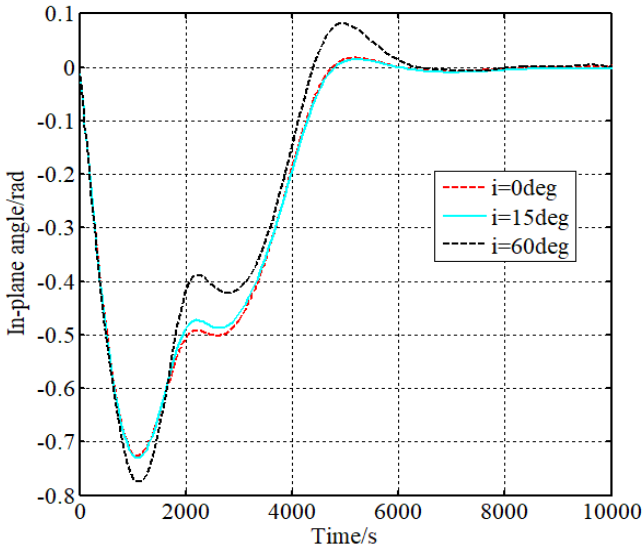

Fig. 5. Variation curves of the in-plane angle versus time

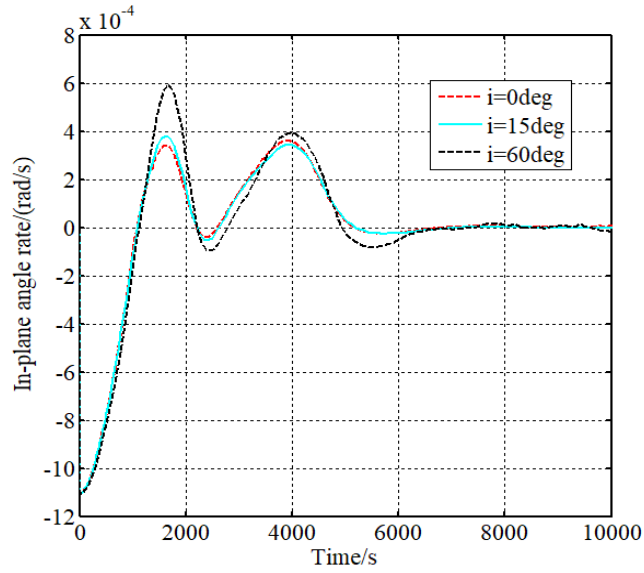

Fig. 6. Variation curves of the in-plane angle rate versus time

Fig. 5 and Fig. 6 demonstrate the changes of the in-plane angle and its rate during tether deployment. As shown in Fig. 5, the in-plane angle in the three cases can eventually converge to zero, which means the EDT system is deployed to the desired local vertical. Fig. 6 shows that the maximum in-plane angle rate occurs at the initial stage, which is accounted for by the action of Coriolis force. The convergence of the in-plane motion takes about 8860s (nearly 1.56 orbital periods), which is a little bit longer than the time needed for the tether length to reach the desired state. This illustrates that the in-plane motion goes on after the tether length is already fully deployed, and for this stage the control mainly depends on adjusting current along the tether within a quite small range, which can be found from the curves of the control inputs shown in the figures below. Besides, it can be seen from the

comparison of the curves that the in-plane angle in the case $i = 60^o$ deviates from the local vertical larger during the deployment, which is because the Ampere force will decrease as the orbital inclination increases. For the same reason, the overshoot of the curve in the case $i = 60^o$ is also larger than that in the other two cases.

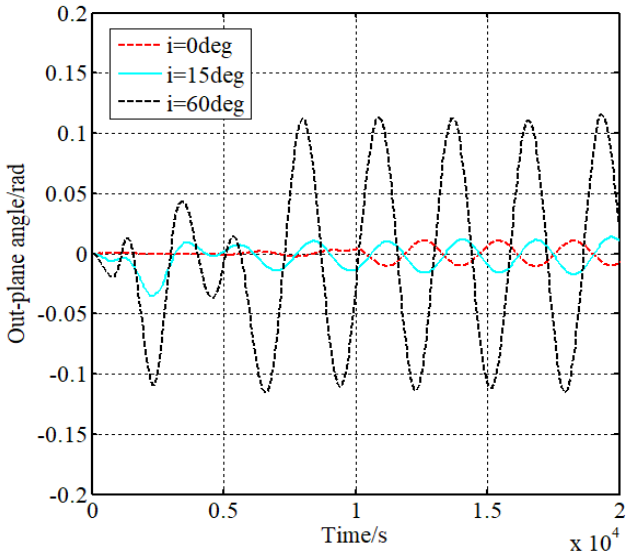

Fig. 7. Variation curves of the out-plane angle versus time

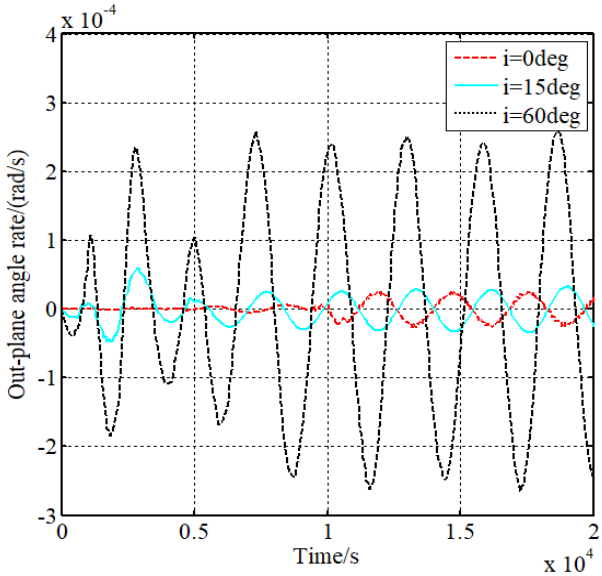

Fig. 8. Variation curves of the out-plane angle rate versus time

Simulation results shown in Fig. 7 and Fig. 8 indicate that the out-plane motion in the three cases is quite tiny during the EDT development. Here, the simulation time is specially extended to 20000s so as to demonstrate the long-term dynamic responses of the out-plane angle well. Particularly, when the EDT system is running in the equatorial plane, the Ampere force will not affect the out-plane motion, which can be seen from the dynamic model

of the system. As the orbital inclination increases, the component of Ampere force on the out-plane motion will strengthen, which results in the enlargement of the amplitude of the out-plane motion.

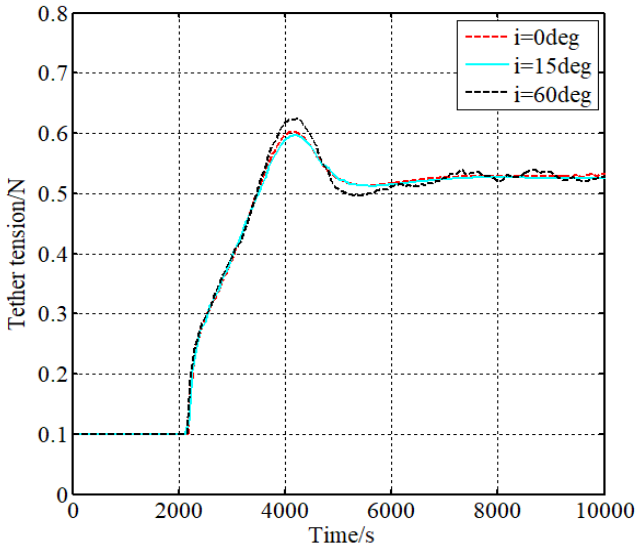

Fig. 9. Variation curves of the tether tension versus time

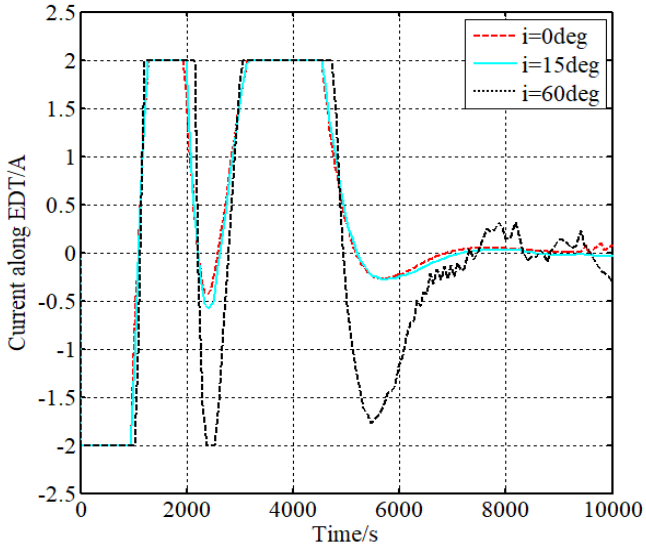

Fig. 10. Variation curves of current along the EDT versus time

Fig. 9 and Fig. 10 depict the time histories of the control inputs in the three cases. Tether tension at the initial stage is restricted to the permissible minimum $0.01\mathrm{N}$, because if tension is smaller or even negative, the tether may not be deployed successfully. It is worth mentioning that, although there is also an upper limit for the tension ($1\mathrm{N}$ given in the cases), such a maximum is never actually reached under the proposed control strategy. When the tether is fully deployed, the curves of the tether tension slightly fluctuate due to the effect of the external disturbances. On the other hand, limits for the current are symmetrical with respect to zero, it is because that the

current direction may be regulated via plasma contactors installed on the end-bodies [25]. Similarly, the curves of the current also fluctuate after tether deployment, and obviously, the amplitude of the current fluctuation in the case of $i = 60^o$ is larger when dealing with the disturbances.

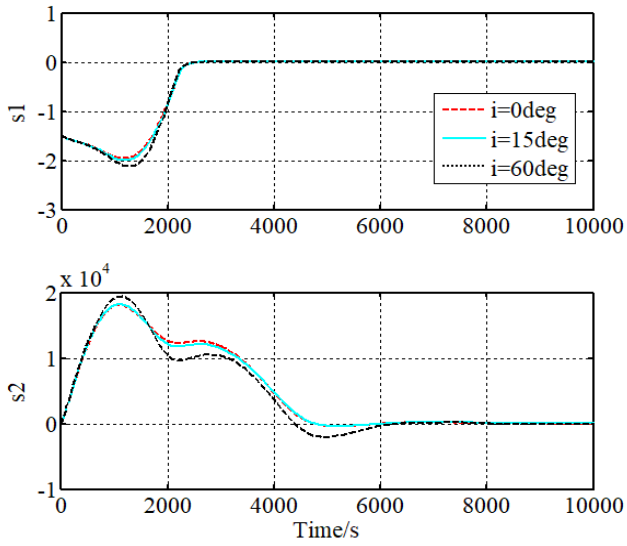

Fig. 11. The sliding mode surfaces versus time

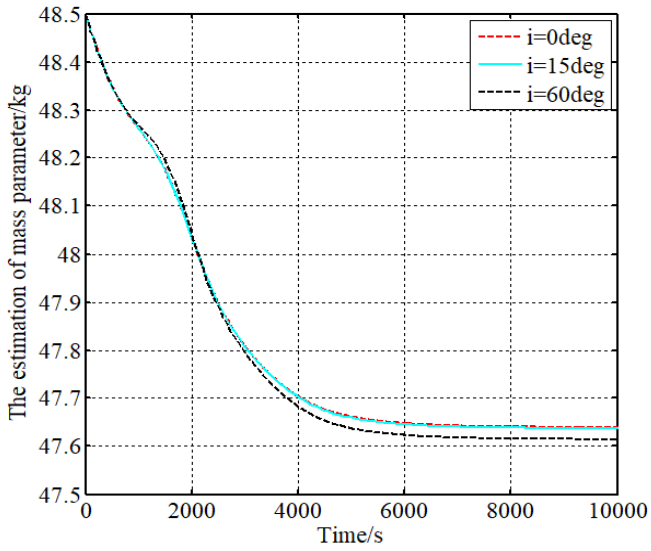

Fig. 12. The estimations of the mass parameter of the system

The curves of the sliding mode surfaces are shown in Fig. 11. As shown in the figure, the sliding surfaces s_1 and s_2 in the cases can converge to zero. Fig. 12 shows the estimation values of the unknown mass parameter in the three cases. The real value of m_e in the cases is equal to 47.619kg . As shown in Fig. 12, the estimations $\hat{m}_e$ calculated by the adaptive law start from the given initial value, and then stabilize at 47.639kg (the red line),

47.628kg (the blue line), and 47.612kg (the black line), respectively. All the estimated results are close to the real value.

4.3 The influence of disturbances and uncertainty

In order to verify the anti-disturbance ability of the proposed hybrid control strategy and the influence of the model uncertainty, more cases are discussed in this subsection, which may illustrate the influence of the initial perturbations, the external disturbances, and the uncertainty of mass parameter in the model.

4.3.1 The influence of the initial perturbations

Considering there may be some perturbations at the initial moment of tether deployment, which may cause deviations in the ejection direction, the comparison below focuses on the impact of the deviations of the initial in-plane angle. When making the comparison for the initial in-plane angle, the other parameters are the same as the previous parameter settings. And the orbital inclination is chosen as $i = 15^o$. The blue lines in the following simulations are chosen as the baselines, which represent variation curves in the case of $\theta(0) = 0\text{rad}$, and the red and black lines depict the cases of $\theta(0) = 0.1\text{rad}$ and $\theta(0) = -0.1\text{rad}$, respectively.

Fig. 13-15 demonstrate the states of the system in the three cases. The results suggest that although the deviations of the in-plane angle will affect the deployment process, the system can reach the desired local vertical, which indicates that the proposed control strategy has the ability to overcome the influence of the initial perturbations. The corresponding control inputs are shown in Fig. 16 and Fig. 17.

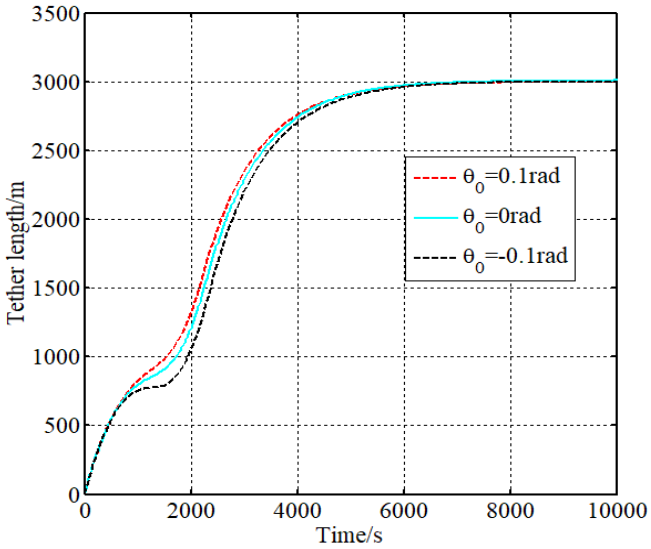

Fig. 13. Variation curves of the tether length versus time

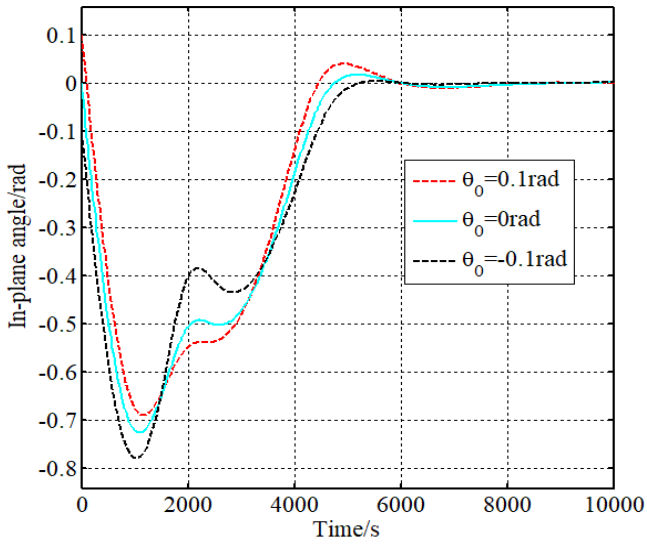

Fig. 14. Variation curves of the in-plane angle versus time

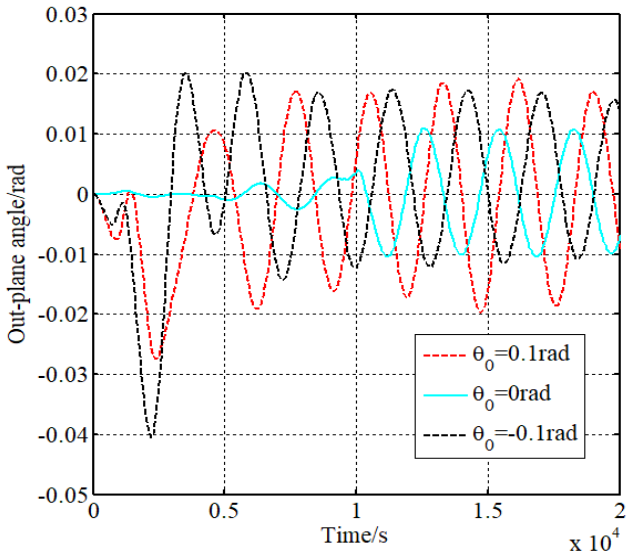

Fig. 15. Variation curves of the out-plane angle versus time

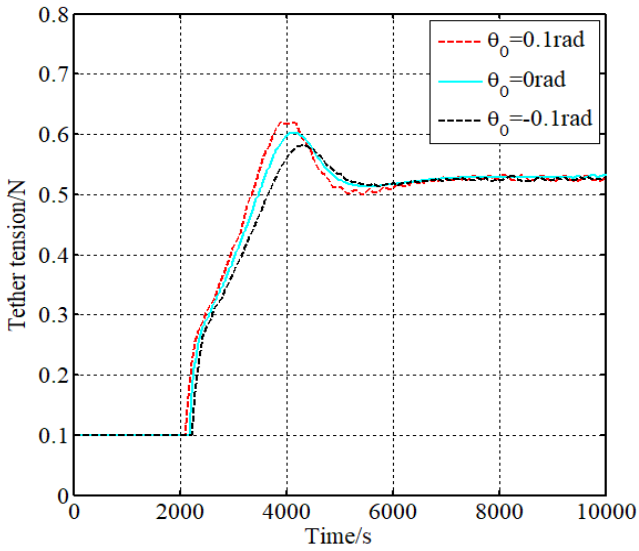

Fig. 16. Variation curves of the tether tension versus time

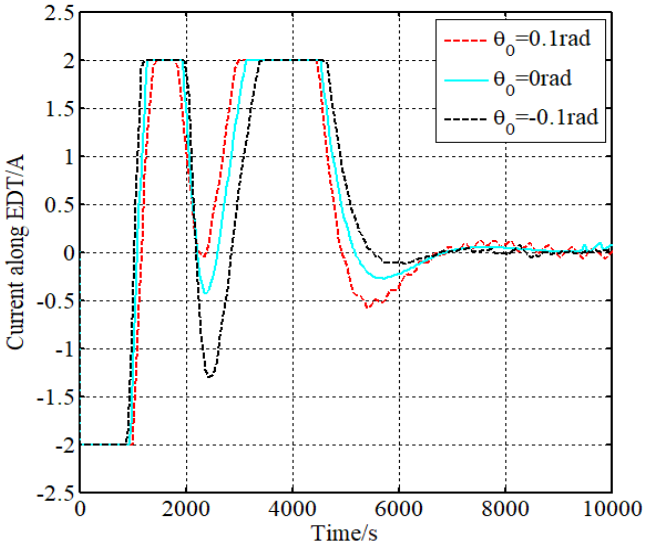

Fig. 17. Variation curves of the current along the tether versus time

4.3.2 The influence of the external disturbances

Note that the magnitude of the external disturbance Δ is too small to verify the effectiveness of the proposed controller, the amplitude of the disturbance in the following simulations is enlarged, which can depict more severe influence. The blue lines in the figures represent the baseline case; the red lines and black lines represent the cases under the enlarged disturbance by 5 times and 10 times, respectively.

Fig. 18-20 show the states of the system in the three cases. As shown in the figures, the EDT system can bear more severe influence than the actual possible disturbances during deployment, which indicates that the proposed control strategy has a strong ability of anti-disturbance. The corresponding control inputs are shown in Fig. 21 and

Fig. 22. It is worth noting that the curves of the tether tension and current slightly fluctuate after the tether is fully deployed due to the influence of the disturbances.

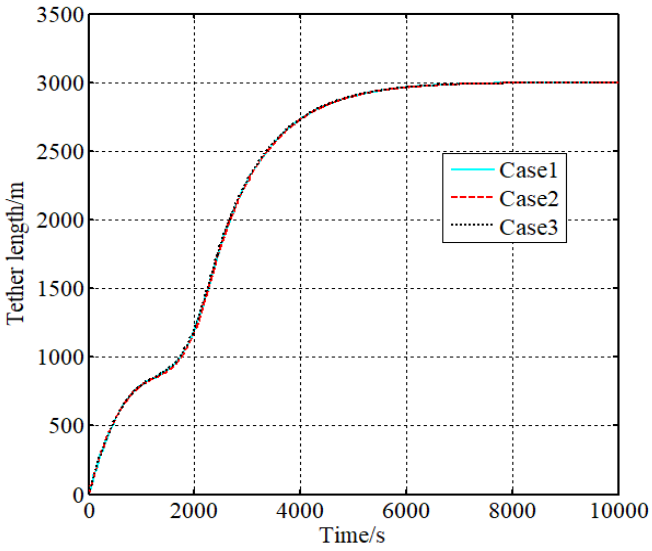

Fig. 18. Variation curves of the tether length versus time

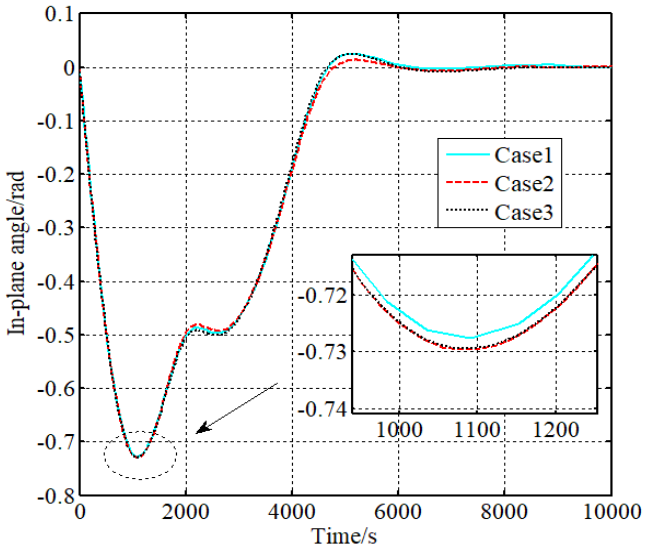

Fig. 19. Variation curves of the in-plane angle versus time

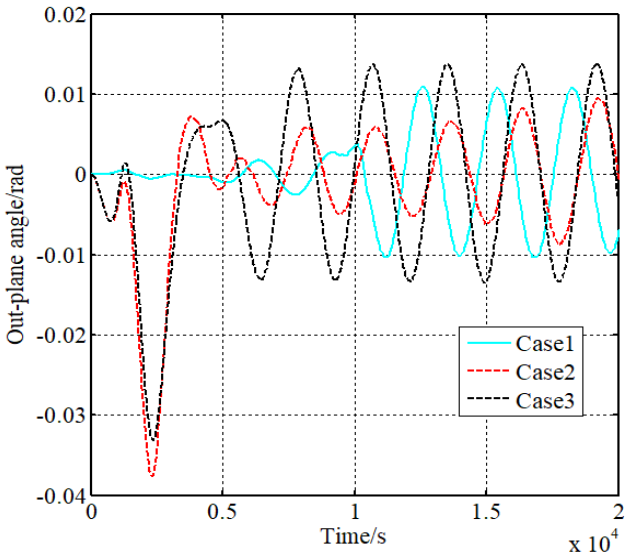

Fig. 20. Variation curves of the out-plane angle versus time

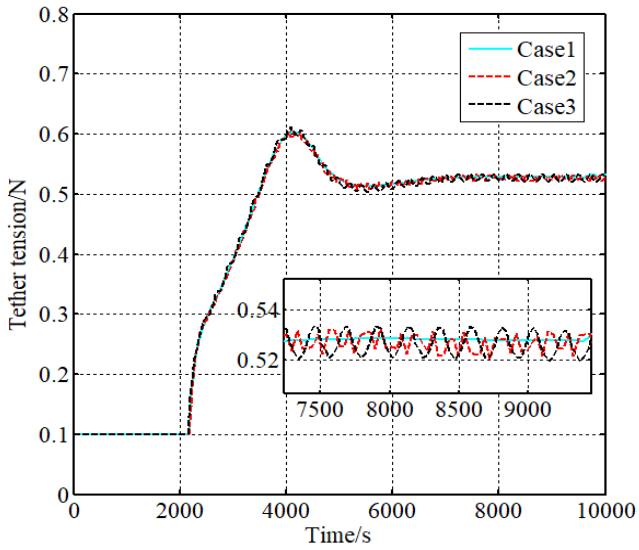

Fig. 21. Variation curves of the tether tension versus time

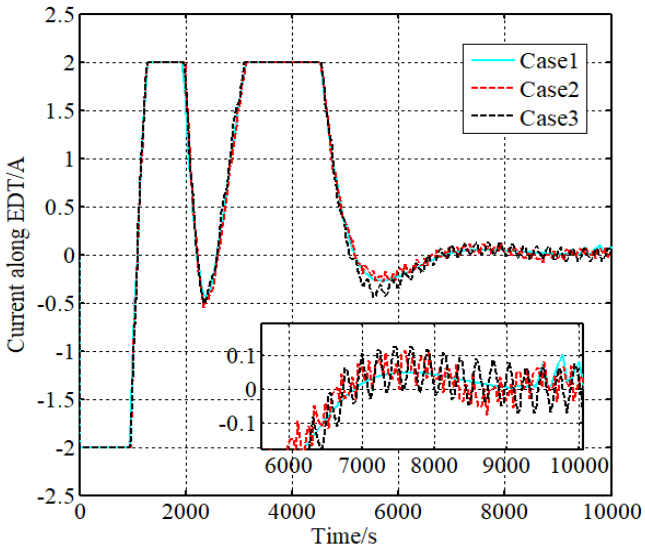

Fig. 22. Variation curves of the current along the tether versus time

4.3.3 The influence of the mass uncertainty

Due to the reasons stated in Sec. 3, the mass parameter of the system m_e may be unknown in the practical missions. The influence of the mass uncertainty can be investigated by varying the value of m_2. It should be noted that owing to the given upper and lower bounds of m_e, the value of m_2 is allowed to vary from $m_2 = 48\text{kg}$ to $m_2 = 52\text{kg}$. For the comparison purpose, the case of $m_2 = 50\text{kg}$ in the following simulations is used as a benchmark. In order to verify the effectiveness of the proposed controller, the other two cases are performed under the condition of $m_2 = 48\text{kg}$ and $m_2 = 52\text{kg}$ respectively, which stand for the extreme cases within the boundary. The other parameters of the system and the disturbances are kept the same as shown in the part of parameter settings.

Fig. 23-25 depict the time histories of the system states. It can be seen that the proposed control strategy is successful in dealing with the uncertainty of the mass parameter in the three cases and achieving the fast and stable deployment in 1.35 orbit periods roughly as discussed in the previous section. Thus, it can be concluded that the uncertainty caused by the unknown mass parameter has no significant effect on the performance of tether deployment in the proposed control law, which reveals the effectiveness of the deployment controller. Besides, it is worth noting that the curves of the tether tension separate from each other and stabilize at different values after the tether is fully deployed due to the difference of the mass parameter in the three cases, as shown in Fig. 26.

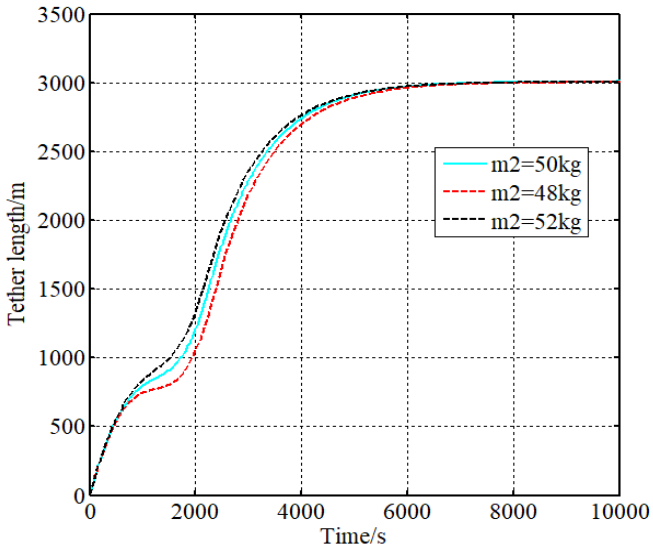

Fig. 23. Variation curves of the tether length versus time

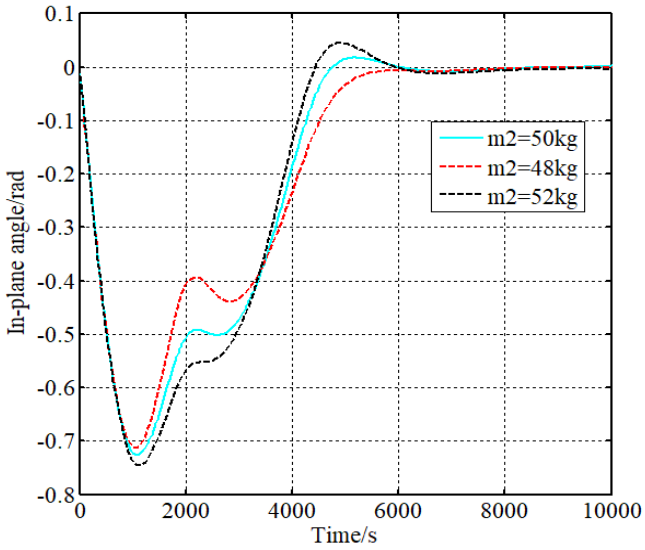

Fig. 24. Variation curves of the in-plane angle versus time

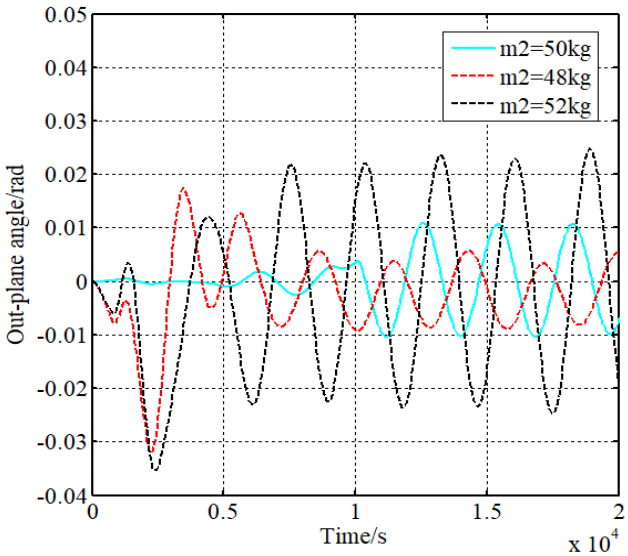

Fig. 25. Variation curves of the out-plane angle versus time

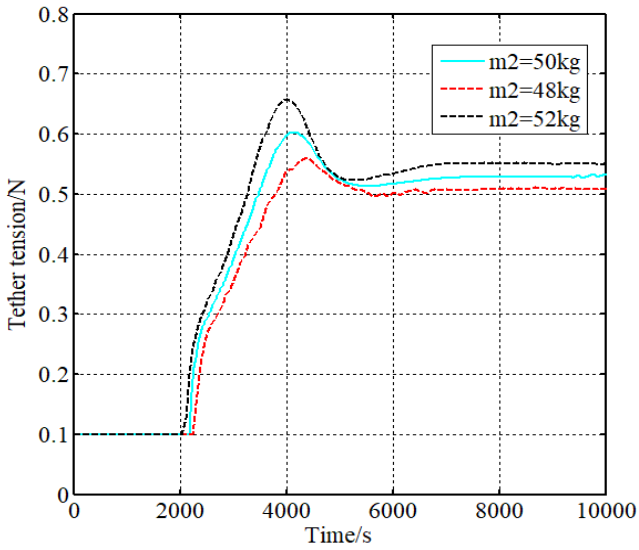

Fig. 26. Variation curves of the tether tension versus time

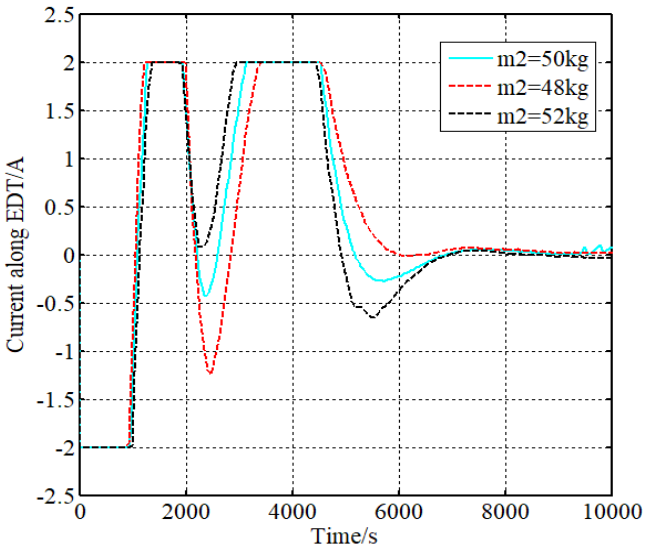

Fig. 27. Variation curves of the current along the tether versus time

5. Conclusions

The present work developed a hybrid controller for the deployment of EDT system by regulating tether tension and electric current simultaneously. In order to address the challenges of the possible disturbances and the uncertainty caused by the unknown mass parameter, the sliding mode control combined with adaptive law is adopted, and the asymptotically stability of the system is proved by the Lyapunov theory. The simulation results show that the EDT system is deployed to the local vertical successfully within 1.35 orbit times roughly without tether winding in the cases of different orbital inclinations, and the proposed adaptive law performs well in estimating the unknown mass parameter of the system. Furthermore, the anti-disturbance ability of the controller is demonstrated by evaluating the influence of the initial ejection perturbations, the external disturbances in different amplitudes and the mass uncertainty. In future studies, nonlinear sliding mode control method, combined with adaptive approach, may provide further insight into the hybrid regulation of tether tension and current for EDT deployment.

Acknowledgements

This work is supported by the Fundamental Research Funds for the Shaanxi Science and Technology Program (No. 2017KW-ZD-04) and China Scholarship Council (N0. 201906290210).

References

[1] H. Wen, D. Jin, H. Hu, Advances in dynamics and control of tethered satellite systems, Acta Mechanica Sinica, 24 (2008) 229-241.

[2] M.P. Cartmell, D.J. Mckenzie, A review of space tether research, Progress in Aerospace Sciences, 44 (2008) 1-21.

[3] K. D. Kumar, Review on dynamics and control of non-electrodynamic tethered satellite systems, Journal of Spacecraft and Rockets, 43 (2006) 705-720.

[4] A. Atashgah, H. Gazerpour, A. Lavaei, et al, An active time-optimal control for space debris deorbiting via geomagnetic field, Celestial Mechanics and Dynamical Astronomy, 128 (2017) 343-360.

[5] R. Qi, A. Shi, A.K. Misra, et al, Coulomb tether double-pyramid formation, a potential configuration for geostationary satellite collocation. Aerospace Science and Technology, 84 (2019) 1131-1140.

[6] P. Williams, In-plane payload capture with an elastic tether, Journal of Guidance, Control, and Dynamics, 29 (2006) 810-821.

[7] H. Kalita, R. Furfaro, J. Thangavelautham, Satellite Capture and Servicing Using Networks of Tethered Robots Supported by Ground Surveillance, Advanced Maui Optical and Space Surveillance Technologies Conference, 2018.

[8] J. R. Sanmartin, A review of electrodynamic tethers for science applications, Plasma Sources Science and Technology, 19 (2010) 1-10.

[9] J. R. Sanmartin, M. Charro, E. C. Lorenzini, et al, Electrodynamic tether at Jupiter—II: fast moon tour after capture, IEEE Transactions on Plasma Science, 37 (2009) 620-626.

[10] D. Xu, X. Kong, Tether modeling study on electro-dynamic tether deorbiting system, Acta Aeronautica Et Astronautica Sinica, 29 (2008) 1196-1201.

[11] J. Pelaez, E. C. Lorenzini, Libration control of electrodynamic tethers in inclined orbit, Journal of Guidance, Control, and Dynamics, 28 (2005) 269-279.

[12] R. Zhong, Z. Zhu, Libration dynamics and stability of electrodynamic tethers in satellite deorbit, Celestial Mechanics and Dynamical Astronomy, 116 (2013) 279-298.

[13] H. Kojima, T. Sugimoto, Nonlinear control of electro-dynamic tether system, Aiaa/aas Astrodynamics Specialist Conference & Exhibit. 2013.

[14] M. InArrea, V. Lanchares, A. I. Pascual, et al, Attitude stabilization of electrodynamic tethers in elliptic orbits by time-delay feedback control, Acta Astronautica, 96 (2014) 280-295.

[15] P. Williams, Optimal deployment/retrieval of a tethered formation spinning in the orbital plane, Journal of Spacecraft & Rockets, 43 (2005) 638-650.

[16] Y. M. Zabolotnov, Control of the deployment of an orbital tether system that consists of two small spacecraft, Cosmic Research, 55 (2017) 224-233.

[17] B. Yu, H. Wen, D. Jin, Review of deployment technology for tethered satellite systems, Acta Mechanica Sinica, 34 (2018) 162-176.

[18] L. Murugathasan, Z. Zhu, Deployment control of tethered space systems with explicit velocity constraint and invariance principle, Acta Astronautica, 157 (2019) 390-396.

[19] H. Wen, Z. Zhu, D. Jin, et al, Space tether deployment control with explicit tension constraint and saturation function, Journal of Guidance Control and Dynamics, 39 (2016) 1-6.

[20] J. Kang, Z. Zhu, W. Wang, et al, Fractional order sliding mode control for tethered satellite deployment with disturbances, Advances in Space Research, 59 (2017) 263-273.

[21] C. Wei, J. Luo, B. Gong, et al, On novel adaptive saturated deployment control of tethered satellite system with guaranteed output tracking prescribed performance, Aerospace Science and Technology, 75 (2018) 58-73.

[22] G. Li, Z. Zhu, S. A. Meguid, Libration and transverse dynamic stability control of flexible bare electrodynamic tether systems in satellite deorbit, Aerospace Science and Technology, 49 (2016) 112-129.

[23] J. Zhang, Z. Zhu, W. Zhao, Reduction of libration angle in electrodynamic tether deployment by Lorentz force, Journal of Guidance Control Dynamics, 40 (2017) 164-169.

[24] J. Huang, G. Liu, D. Zhu, et al, Current and tension control for deployment of a deorbiting electro-dynamic tether system, Acta Aeronautica Et Astronautica Sinica, 39 (2018) 1-10.

[25] H. Wen, D. Jin, H. Hu, Three-dimensional deployment of electro-dynamic tether via tension and current control with constraints, Acta Astronautica, 129 (2016) 253-259.

[26] C. Luo, W. Hao, D. Jin, Libration control of bare electrodynamic tether for three-dimensional deployment, Astrodynamics, 2 (2018) 187-199.

[27] M. Kruijff, E. van der Heide, W. Ockels, et al, First Mission Results of the YES2 Tethered SpaceMail Experiment, AIAA/AAS Astrodynamics Specialist Conference and Exhibit. 2008.

[28] E. M. Levin, Dynamic Analysis of Space Tether Missions, first ed., Univelt, San Diego, USA, 2007. pp 123.

[29] L. Xu, B. Yao, Adaptive robust control of mechanical systems with non-linear dynamic friction compensation, International Journal of Control, 81(2) (2008) 167-176.

[30] Z. Ma, G. Sun, Z. Li, Dynamic adaptive saturated sliding mode control for deployment of tethered satellite system, Aerospace Science and Technology, 66 (2017) 355-365.

[31] X. Xin, Y. Liu, Control Design and Analysis for Underactuated Robotic Systems, first ed., Springer-Verlag, London, 2014.

Highlights

- A hybrid deployment strategy for the electro-dynamic tether is investigated.
- The tether is deployed to the desired local vertical via limited tension and current regulation.
- The deployment controller has a strong ability of anti-disturbance.
- The unknown mass parameter of the system is well-estimated using the adaptive law.